CHAPTER 1

INTRODUCTION

1.1 Background

It is well known that rare-earth oxides have been applied widely in many fields. Among them, cerium dioxide or ceria (CeO_2) finds numerous applications in catalysts, catalyst supports cosmetics materials, chemical-mechanical polishing (CMP), ceramic materials, oxygen gas sensors, solid oxide fuel cells, UV absorbents and fluorescent materials [1-5] . Moreover, nano-sized materials have been studied vigorously in recent years because their significant properties are different from the bulk.

Therefore, the studies on the preparation and properties of CeO_2 nanocrystalline have attracted extensive interests during the last few years. CeO_2 nanocrystalline has been prepared by sol-gel process [2], sonochemical synthesis [3], Thermal Decomposition [4] and hydrothermal synthesis [5]. In the sol-gel process, alkoxide or organometallic compounds are usually used as precursors. However, the expensive cost of precursor materials and more complicated reaction mechanism often restrict the potential use of sol-gel process. Besides, the reactions for hydrothermal synthesis and forced hydrolysis are often carried out under much severer conditions, such as higher temperature, higher pressure, and longer reaction time. These methods have defects in the complex process and expensive raw materials, so the cost of production is very high and it is difficult to be realized in industrial production [1].

Compared to these methods, the homogeneous precipitation demonstrates promising development in fabricating CeO_2 nanoparticles due to advantages of low cost, mild synthesis condition and easy scale-up. The addition of low dielectric medium to the aqueous solution can alter the thermodynamics of reaction system and nucleation kinetics, which would result in reducing the particle size and size distribution of resulting particles [6].

Recently, some alkali-layered metal oxide photocatalysts were suggested as highly photosensitive photocatalysts to improve the photocatalytic activity [8]. Photocatalytic reduction is mainly used for the removal of the dissolved metal ions by reducing them to their insoluble forms. A widely investigrated inorganic ion is the carcinogenic Cr(VI) anions. Other inorganic compound investigated in photoreduction include Hg(II), Cd(II), and Ag(I). The presence of noble metals on semiconductor alters the semiconductor surface properties. Figure 1, illustrates the ability of Ag, a noble metal in contact with a semiconductor surface, to capture electrons. Upon excitation, electrons can migrate to the metal deposit where they can be trapped or captured by an oxidant (A^+). The hole is then free to migrate to the surface where oxidation can occur ($D \rightarrow D^+$).

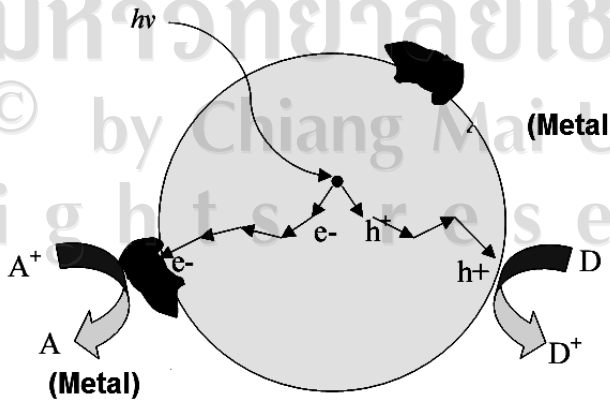

Figure 1.1 Electron mediation by metal in contact with a semiconductor surface

In this work, pure CeO_2 and Ag-doped CeO_2 nanoparticles were synthesized by the homogeneous precipitation method and the impregnation method, respectively. Pure CeO_2 and Ag-doped CeO_2 nanoparticles were characterized by using X-ray diffraction (XRD), Scanning Electron Microscopy (SEM), energy-dispersive spectrometry (EDS), Transmission Electron Microscopy (TEM) and nitrogen adsorption (BET analysis) analyses. XRD was used to confirm the phase and crystalline structure of pure CeO_2 and Ag-doped CeO_2 nanoparticles. SEM and EDS were used to analyze morphology and chemical compositions of pure CeO_2 and Ag-doped CeO_2 nanoparticles. TEM was selected to determine the accurate size and morphology. BET was used to evaluate the specific area of pure CeO_2 and Ag-doped CeO_2 nanoparticles. The photocatalytic activity of pure CeO_2 and Ag-doped CeO_2 nanoparticles were investigated and the effect of silver on the photocatalytic activity of CeO_2 was studied.

1.2 Cerium dioxide (CeO_2) [9-12]

Cerium(IV) oxide, ceric oxide, ceria, or sometimes simply cerium oxide or cerium dioxide, is a pale yellow-white powder, CeO_2. It is used in ceramics, to polish glass, and to sensitize photosensitive glass. It is also used in lapidary as "jeweller's rouge"; it is also known as "optician's rouge".[1] Ceria is used in the walls of self-cleaning ovens as a hydrocarbon catalyst during the high-temperature cleaning process. It has high absorption of ultraviolet radiation while it is transparent for visible light, so it is a prospective replacement of zinc oxide and titanium dioxide in sunscreens, as it has lower photocatalytic activity. However its thermal catalytic properties have to be decreased by coating the particles with amorphous silica or

boron nitride. Powdered ceria is slightly hygroscopic and will also absorb a small amount of carbon dioxide from the atmosphere.

The crystal structure of CeO_2 is fluorite structure. The cerium atoms (Ce^{4+}) are 8 coordinate and the oxygen atoms (O^{2-}) are 4 coordinate. In this struture Ce atom is surrounded by 8 oxygen neighboring at corners of slightly distorted tetrahedral as shown in Figure 1.2 [11]. The chemical and physical properties of CeO_2 are shown in Table 1.1

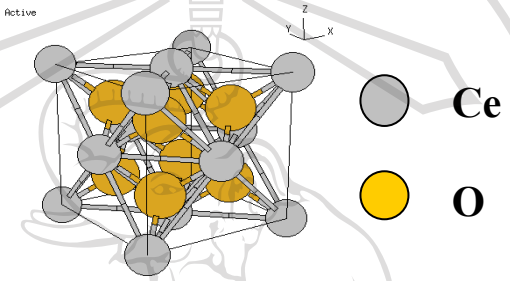

Figure 1.2 The Crystallograpic structure of CeO_2 in cubic phase [11]

Table 1.1 Chemical and physical properties of CeO_2 [9-10]

Property	**Value**
IUPAC name	Cerium(IV) oxide
Other names	ceric oxide, ceria, cerium oxide, cerium dioxide
Molecular formula	CeO_2
Structure	fluorite structure
Molecular weight	172.115 g/mol
Appearance	white or pale yellow solid, slightly hygroscopic
Melting point	Approximately 2,400 K (2,100 °C)
Boiling point	3,500 °C
Density	7.65 g/cm^3
Solubility in water	insoluble

1.3 Silver (Ag) [13]

Silver is a chemical element with the chemical symbol Ag and atomic number 47. A soft, white, lustrous transition metal, it has the highest electrical conductivity of any element and the highest thermal conductivity of any metal. The metal naturally occurs in its pure, free form (native silver) and as an alloy with gold (electrum), as well as in various minerals, such as argentite and chlorargyrite. Most silver is produced as a by-product of copper, gold, lead, and zinc refining.

Silver has been known since ancient times and has long been valued as a precious metal, used to make ornaments, jewellery, high-value tableware and utensils (hence the term *silverware*) and currency coins. Today, silver metal is used in electrical contacts and conductors, in mirrors and in catalysis of chemical reactions. Its compounds are used in photographic film and dilute solutions of silver nitrate and other silver compounds are used as disinfectants. Although the antimicrobial uses of silver have largely been supplanted by the use of antibiotics, further research into its clinical potential is in progress.

Silver is a very ductile and malleable (slightly harder than gold) monovalent coinage metal with a brilliant white metallic luster that can take a high degree of polish. It has the highest electrical conductivity of all metals, even higher than copper, but its greater cost and tarnishability have prevented it from being widely used in place of copper for electrical purposes, though 13540 tons were used in the electromagnets used for enriching uranium during World War II (mainly because of the wartime shortage of copper). Another notable exception is in high-end audio cables.

Among metals, pure silver has the highest thermal conductivity, the whitest color, and the highest optical reflectivity. Silver also has the lowest contact resistance of any metal. Silver halides are photosensitive and are remarkable for their ability to record a latent image that can later be developed chemically. Silver is stable in pure air and water, but tarnishes when it is exposed to air or water containing ozone or hydrogen sulfide. The most common oxidation state of silver is +1 (for example, silver nitrate: $AgNO_3$); in addition, +2 compounds (for example, silver(II) fluoride: AgF_2) and +3 compounds (for example, potassium tetrafluoroargentate: $K[AgF_4]$) are known. The chemical and physical properties of silver are shown in Table1.2

Table 1.2 Chemical and physical properties of silver [13]

Property	**Value**
Name, Symbol, Number	Sliver (Ag)
Atomic number	47
Structure	Cubic face centered
Molecular weight	107.8682 $g \cdot mol^{-1}$
Density	10.49 $g.cm^{-3}$
Melting point	961.78 °C
Boiling point	2162 °C
Atomic radius	160 pm
Covalent radius	153 pm
Thermal conductivity	429 $W \cdot m^{-1} \cdot K^{-1}$ at 300K)
Electronic shell	[Kr] $4d^{10}$ $5s^{1}$

1.4 Powder preparation

1.4.1 Sol-gel method [2, 14, 15]

The sol-gel process allows synthesizing ceramic materials of high purity and homogeneity by mean of preparation techniques different from the traditional process of fusion of oxides. This process occurs in liquid solution of organometallic precursors which, by means of hydrolysis and condensation reactions, lead to the formation of a new phase (sol). The reaction schemes were described by reaction (1.1)-(1.3)

$$M\text{-}O\text{-}R + H_2O \rightarrow M\text{-}OH + R\text{-}OH \text{ (hydrolysis)} \quad (1.1)$$

$$M\text{-}OH + HO\text{-}M \rightarrow M\text{-}O\text{-}M + H_2O \text{ (water condensation)} \quad (1.2)$$

$$M\text{-}O\text{-}R + HO\text{-}M \rightarrow M\text{-}O\text{-}M + R\text{-}OH \text{ (alcohol condensation)} \quad (1.3)$$

The sol is made of solid particles of diameter of few hundreds nm suspended in a liquid phase. Then the particles condense in a new phase (gel) in which a solid macromolecule is immersed in a liquid phase (solvent). Drying the gel by means of low temperature treatments (25-100^{o}C), it is possible to obtain porous solid matrices.

The fundamental property of the sol-gel process is that it is possible to generate ceramic material at a temperature close to room temperature. Therefore such a procedure opened the possibility of incorporating glasses soft dopants, such as fluorescent dye molecules and organic chromophores into ceramic substrates.

1.4.2 Precipitation method [1, 6-8, 16, 17, 18]

The precipitation process usually follows by adjusting pH, adds chemicals to facilitate stimulate precipitation, adds coagulants, and mixes the fluid in a device called a flocculator. The chemical precipitants, coagulants, and flocculants are all used to increase the particle size through aggregation. The commonly used

precipitants include carbonates, sulfates, sulfides, lime and other hydroxides. The precipitants generate very fine particles that are held in suspension. Coagulants are often added to aggregate the suspended particles. Mixing in a flocculator following the addition of coagulants promotes contact between the particles, which in turn promotes particle growth and settling.

1.4.3 Hydrothermal method [5, 19, 20, 21]

The original hydrothermal method involves heating the reaction in a closed vessel (an autoclave) with water. In a closed vessel the pressure increases and the water remains liquid above its normal boiling temperature of 100^{o}C. These conditions, in which the temperature is raised above boiling temperature of water and the pressure raised above atmosphere pressure, are known as hydrothermal conditions. Powders prepared via hydrothermal method are often unagglomerated, anhydrous and crystalline. Consequently, the prepared powders do not have to be calcined or milled. They remain unagglomerated and substantially free of impurities.

Hydrothermal synthesis offers a potentially superior technique for low cost and low temperature production of piezoelectric materials. Normally, hydrothermal synthesis has been used for preparing ceramic powders for a variety of applications. It has superiority over the other powder preparation methods in that high calcinations temperature is not necessary for the synthesis of crystallized ceramic powders.

1.4.4 Thermal decomposition method [4, 22-24]

Thermal decomposition is defined as a chemical reaction whereby a chemical substance breaks up into at least two chemical substances when heated. It is usually an endothermic reaction as heat is required to break chemical bonds in the compound undergoing decomposition. *Thermolysis* (from *thermo-* meaning heat and -lysis

meaning break down) is a chemical process by which a substance is decomposed into other substances by use of heat. The decomposition temperature of a substance is the temperature at which the substance decomposes into smaller substances or into its constituent atoms. High temperatures can also induce polymerization, which produces larger molecules, possibly also causing thermal decomposition and evaporation of smaller molecules in the process.

1.4.5 Impregnation mathod [25, 26]

Impregnation method is considered as a simple method of making a catalyst. The powder of catalyst is contacted with a solution then dried and calcined. The impregnation technique requires less equipment since the filtering and forming steps are eliminated and washing may not require. It is a preferred method in preparing metal ions coating on surface of semiconductors such as TiO_2, ZnO, and SnO_2 due to its simplicity.

1.5 Characterization techniques

1.5.1 Thermal analysis

Thermal analysis is a branch of materials science where the properties of materials are studied as they change with temperature Several methods are commonly used - these are distinguished from one another by the property which is measured such as Differential scanning calorimetry (DSC), Thermogravimetric analysis (TG)

1.5.1.1 Calcination

Calcination (also referred to as calcining) is a thermal treatment process applied to ores and other solid materials in order to bring about a thermal decomposition, phase transition, or removal of a volatile fraction. The calcination

process normally takes place at temperatures below the melting point of the product materials. Calcination is to be distinguished from roasting, in which more complex gas-solid reactions take place between the furnace atmosphere and the solids, as calcination takes place in the absence of air.

1.5.1.2 Thermogravimetric Analysis (TG)

Thermogravimetric analysis (TG) is an analytical technique used to determine a material's thermal stability and its fraction of volatile components by monitoring the weight change that occurs as a specimen is heated. The measurement is normally carried out in air or in an inert atmosphere, such as Helium or Argon, and the weight is recorded as a function of increasing temperature. Sometimes, the measurement is performed in a lean oxygen atmosphere (1 to 5% O_2 in N_2 or He) to slow down oxidation. In addition to weight changes, some instruments also record the temperature difference between the specimen and one or more reference pans (differential thermal analysis, or DTA) or the heat flow into the specimen pan compared to that of the reference pan (differential scanning calorimetry, or DSC). The latter can be used to monitor the energy released or absorbed via chemical reactions during the heating process. In the particular case of carbon nanotubes, the weight change in an air atmosphere is typically a superposition of the weight loss due to oxidation of carbon into gaseous carbon dioxide and the weight gain due to oxidation of residual metal catalyst into solid oxides.

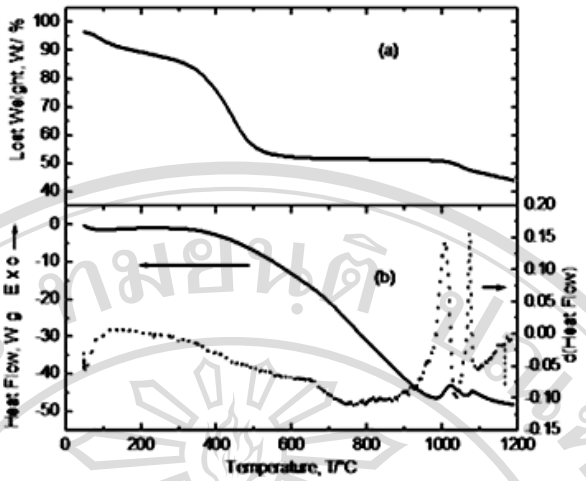

Figure 1.3 Thermogram of Thermogravimetric Analysis

1.5.1.3 Differential scanning calorimetry (DSC)

Differential scanning calorimetry (DSC) is a technique for measuring the energy necessary to establish a nearly zero temperature di®erence between a substance and an inert reference material, as the two specimens are subjected to identical temperature regimes in an environment heated or cooled at a controlled rate.

There are two types of DSC systems in common use (Figure 1.4). In power-compensation DSC the temperatures of the sample and reference are controlled independently using separate, identical furnaces. The temperatures of the sample and reference are made identical by varying the power input to the two furnaces; the energy required to do this is a measure of the enthalpy or heat capacity changes in the sample relative to the reference.

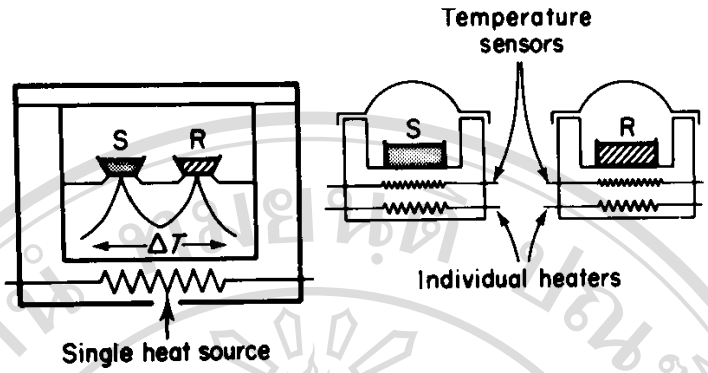

Figure 1.4 (a) Heat flux DSC, (b) power-compensation DSC

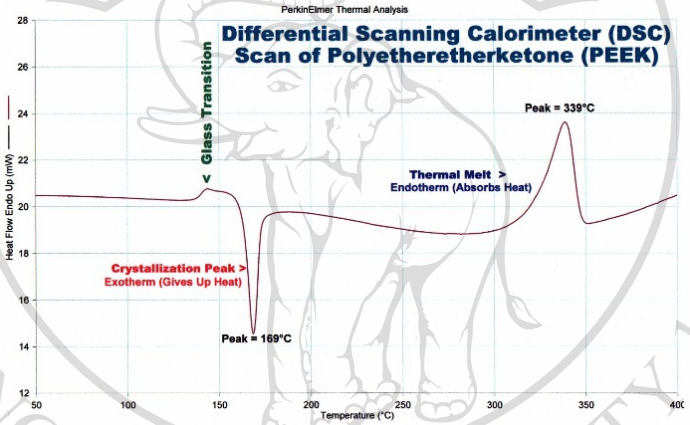

Figure 1.5 Thermogram of DSC

1.5.2 X-ray diffraction method [27-29]

X-ray diffraction is a convenient method to identify an unknown specimen by determining its crystal structure and comparing it with a repository of standard powder diffraction patterns. Exact matching of the interplanar spacings (*d values*) and intensities of all peaks between the standard and an observed diffraction patterns confirms the identity of the unknown as the same as the standard or reference material.

1.5.2.1 The advantage of X-ray diffraction method

The simplicity and advantages of the powder diffraction method for identification of an unknown substance are as follows:

- The powder diffraction pattern is determined by the exact atomic arrangement in a material, so it is like a "fingerprint" of the material.
- Each substance in a mixture produces its own characteristic diffraction pattern independently of the others.
- The X-ray diffraction pattern discloses the presence of a substance as that substance actually exists in the specimen.
- Only a small amount of the material is required for recording the X-ray diffraction pattern.
- The method is nondestructive.

1.5.2.2 Identification of crystal structure by XRD

The X-ray diffraction pattern is a fingerprint of any substance, it should be possible to unambiguously identify that material from its X-ray diffraction pattern. A large collection of X-ray diffraction pattern from a number of substances are available, then the unknown material can be identified by obtaining its diffraction pattern and then determining which pattern from the collection matches exactly with the library diffraction pattern. The Powder Diffraction File (PDF) organized by the Joint Committee on Powder Diffraction Standards (JCPDS), later renamed the International Centre for Diffraction Data (ICDD), and at present collections of nearly 80,000 standard diffraction patterns.

1.5.2.3 Theoretical considerations

Solid matter can be described as amorphous, which the atoms are arranged in a random way similar to the disorder found in a liquid. Glasses are amorphous materials. It can be described as crystalline, which the atoms are arranged in a regular pattern, and there is as smallest volume element that by repetition in three dimensions describes the crystal. The smallest volume element is called a unit cell. The dimension of the unit cell is described by three axes: a, b, c and the angles between them alpha, beta and gamma. About 95% of all solids can be described as crystalline.

An electron in an alternating electromagnetic field will oscillate with the same frequency as the field. When an X-ray beam hits an atom, the electrons around the atom start to oscillate with the same frequency as the incoming beam. In almost all directions will also have destructive interference, that is, the combining waves are out of phase and there is no resultant energy leaving the solid sample. However the atoms in a crystal are arranged in a regular pattern, and in a very few directions will have constructive interference. The waves will be in phase and there will be well defined X-ray beams leaving the sample at various directions. Hence, a diffracted beam may be described as a beam composed of a large number of scattered rays mutually reinforcing one another.

This model is rather complex to handle mathematically. The X-ray reflections from a series of parallel planes inside the crystal. The orientation and interplanar spacings of these planes are defined by the three integers h, k, l called indices. A given set of planes with indices h, k, and l cut the a-axis of the unit cell in h sections, the b-axis in k sections and the c-axis in l sections. A zero indicates that the planes are

parallel to the corresponding axis. In general, the 2, 2, 0 planes cut the a–axis and the b–axis in half, but are parallel to the c–axis as shown in Figure 1.6

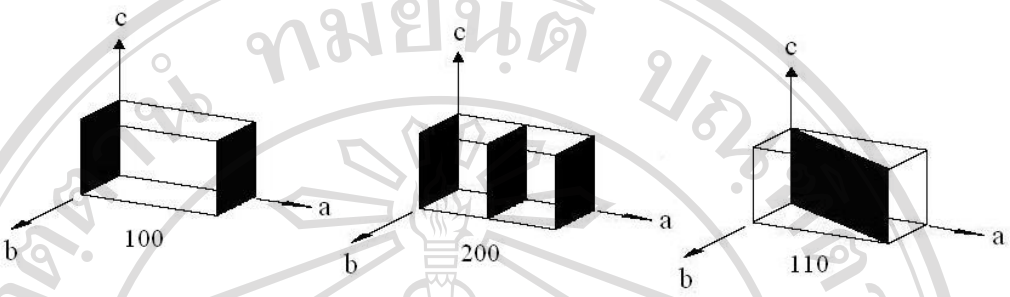

Figure 1.6 The determination of indices of plane [28]

The three dimensional diffraction grating as a mathematical model, the three indices h, k, l become the order of diffraction along the unit cell axes a, b and c respectively. It should now be clear that, depending on what mathematical model has a in mind, the terms X-ray reflection and X-ray diffraction as synonyms. An X-ray beam incident on a pair of parallel planes P1 and P2, separated by an interplanar spacing d as shown in Figure 1.7.

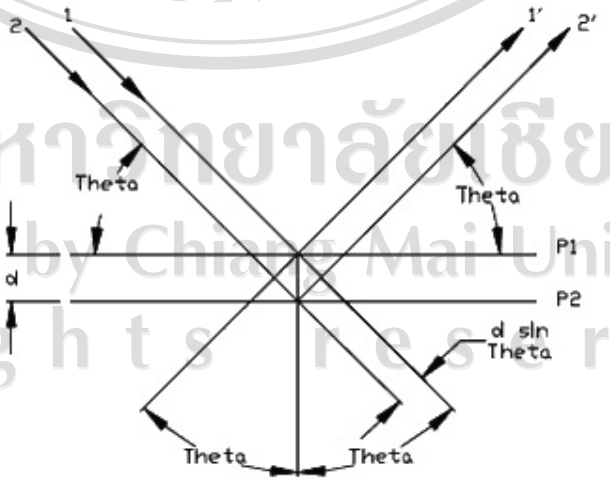

Figure 1.7 Diffraction of X-ray by a crystal [28]

The two parallel incident rays 1 and 2 make an angle (θ) with these planes. A reflected beam of maximum intensity will result if the waves represented by $1'$ and $2'$ are in phase. The difference in path length between1 to $1'$ and 2 to $2'$ must then be an integral number of wavelengths, (λ). The relationship mathematically in Bragg's law is shown in equation 1.4.

$$\mathbf{2d\sin\theta = n\lambda} \qquad (1.4)$$

The process of reflection is described here in terms of incident and reflected (or diffracted) rays, each making an angle θ with a fixed crystal plane. Reflections occur from planes set at angle θ with respect to the incident beam and generates a reflected beam at an angle 2θ from the incident beam. The possible d-spacing defined by the indices h, k, l are determined by the shape of the unit cell. Rewriting Bragg's law is shown in equation 1.5:

$$\mathbf{\sin\theta = \lambda/2d} \qquad (1.5)$$

Therefore the possible 2θ values where reflections are determined by the unit cell dimensions. However, the intensities of the reflections are determined by the distribution of the electrons in the unit cell. The highest electron density is found around atoms. The intensities depend on what kind of atoms exists and where in the unit cell of atoms are located. Planes going through areas with high electron density will reflect strongly, planes with low electron density will give weak intensities.

1.5.2.4 Particle size measurement by XRD

For good quality crystalline material of dimension 0.1 nm is made up of approximately 1,000,000 crystal planes (assuming that d_{hkl} = 1 nm). When an X-ray collides with these planes close to the Bragg angle, diffraction intensity is not

observed because the X-rays reflected from the multitude of parallel planes annihilate one another. With such materials diffraction peaks are produced only within a very narrow window very close to the Bragg angle. Particle sizes are often in the range 1-100 nm for heterogeneous catalysts. In such circumstances the number of stacked planes per particle is in the range of 5-100. This results in the broadening of the XRD peaks because there are insufficient reflecting planes to annihilate phase reflection at angle that are fairly far and removed from the Bragg angle.

This effect has been quantified as the Scherrer equation:

$$t_{hkl} = K\lambda / B_{hkl} \cos\theta_{hkl} \qquad (1.6)$$

Where:

t_{hkl} is the particle size measured from X-rays diffracted from the (*hkl*) planes

B_{hkl} is the full-width at half-maximum (FWHM) of the peak measured in radian from the (*hkl*) planes, $\pi_{radians} = 180^{o}$

θ_{hkl} is the Bragg angle for the reflection from the (*hkl*) planes

K is a constant which depends to some extent on the particles shape. For spherical particles $K = 0.9$.

Figure 1.8 demonstrates how particle size and shape can be determined by XRD analysis. A sample was analyzed by XRD and exhibited the pattern shown, namely one very narrow line and another rather broad. In this case the apparent conflict is caused by the shape of particle. X-rays reflected from the (100) planes, a large particle and a narrow line results. X-rays reflected from the (001) planes, a small particle and a broad line results.

When measuring particles size using XRD line broadening it is important to realize that not all the broadening is due to the particle size effect. Near perfect

crystals should produce extremely narrow XRD lines, but even here some broadening occurs because of instrumental factors. Instrumental contribution to line broadening should be subtracted out by running the XRD of a good quality polycrystalline sample vs the same materials.

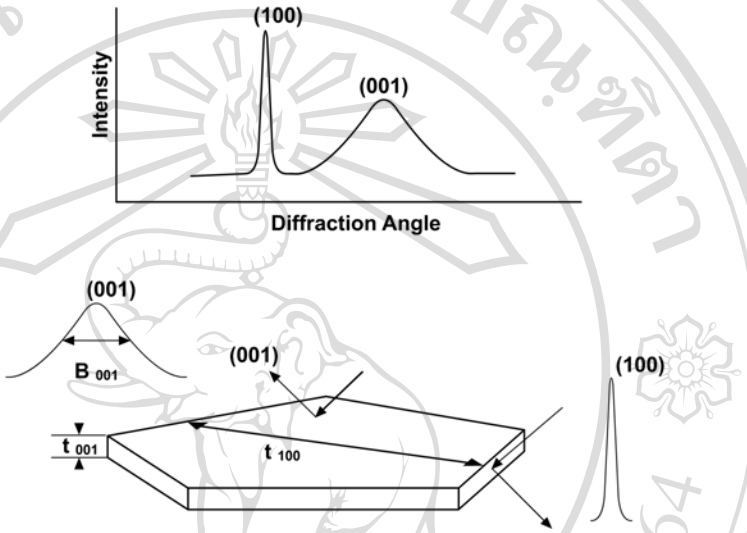

Figure 1.8 Schematic diagram of X-ray line broadening effects [29]

1.5.2.5 Sample preparation

In X-ray diffraction work, normally distinguishes between single crystal and polycrystalline or in powder applications. The single crystal sample is a perfect (all unit cells aligned in a perfect extended pattern) crystal with a cross section of about 0.3 mm. The single crystal diffractometer and associated computer package is used mainly to elucidate the molecular structure of novel compounds, either natural products or man made molecules. Powder diffraction is mainly used for "finger print identification" of various solid materials, e.g. asbestos, quartz.

In powder or polycrystalline diffraction it is important to have a sample with a smooth plane surface. If possible, grinding the sample was normally performed down to particles of about 0.002 mm to 0.005 mm in cross section. The ideal sample is

homogeneous and the crystallites are randomly distributed (problems which will occur if the specimen deviates from this ideal state will be pointed out later). The sample is pressed into a sample holder so that a smooth flat surface is obtained. Ideally, it should be a random distribution of all possible h, k, l planes. Only crystallites having reflecting planes (h, k, l) parallel to the specimen surface will contribute to the reflected intensities. In a truly random sample, each possible reflection from a given set of h, k, l planes will have an equal number of crystallites contributing to it. The sample needs to be fixed through the glancing angle θ in order to produce all possible reflections.

1.5.3 Scanning Electron Microscopy (SEM) [30-32]

The scanning electron microscope (SEM) is a type of electron microscope that creates various images by focusing a high energy beam of electrons onto the surface of a sample and detecting signals from the interaction of the incident electrons with the sample's surface. The type of signals gathered in an SEM varies and can include secondary electrons, characteristic X-rays, and back scattered electrons. In an SEM these signals come not only from the primary beam impinging upon the sample, but from other interactions within the sample near the surface. The SEM is capable of producing high-resolution images of a sample surface in its primary use mode, secondary electron imaging. Due to the manner in which this image is created, SEM images have great depth of field yielding a characteristic three-dimensional appearance useful for understanding the surface structure of a sample. This great depth of field and the wide range of magnifications are the most familiar imaging mode for specimens in the SEM. Characteristic X-rays are emitted when the primary

beam causes the ejection of inner shell electrons from the sample and are used to tell the elemental composition of the sample. The back-scattered electrons emitted from the sample may be used alone to form an image or in conjunction with the characteristic X-rays as atomic number contrast clues to the elemental composition of the sample as shown in Figure 1.9.

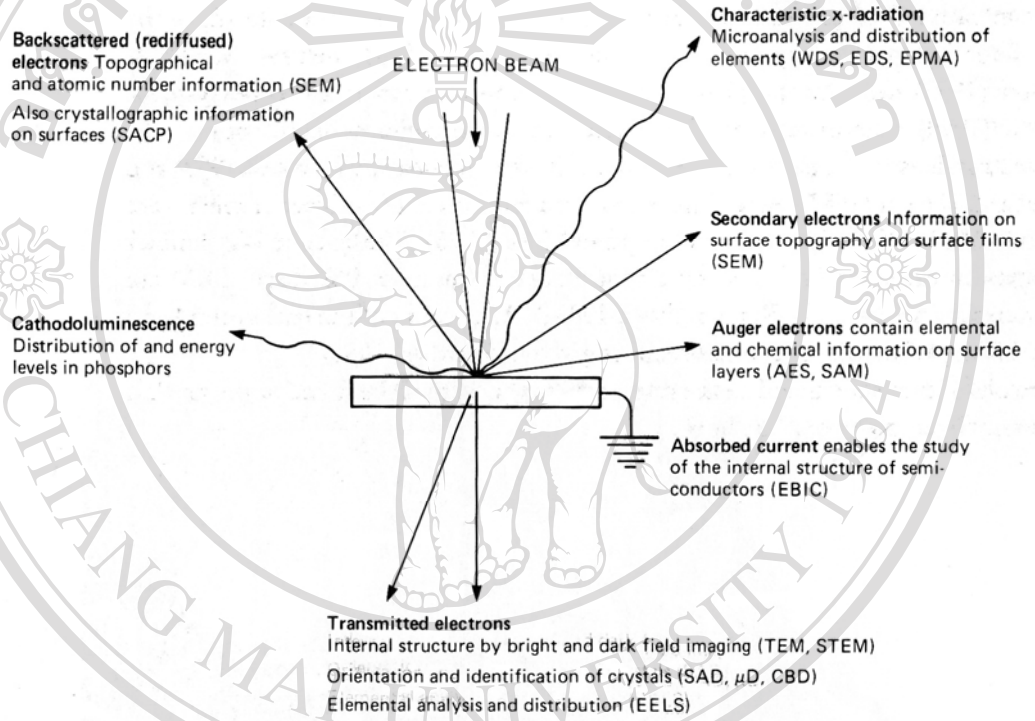

Figure 1.9 Schematic representation of the information resulting from the interaction between the electron beam and the specimen in an electron microscope [30]

1.5.3.1 Detection of secondary electrons

The most common imaging mode monitors low energy (<50 eV) is secondary electrons. Due to their low energy, these electrons originate within a few nanometers from the surface. The electrons are detected by an Everhart-Thornley detector which is a typical of scintillator-photomultiplier device and the resulting signal is rendered into a two-dimensional intensity distribution that can be viewed and saved as a digital

image. This process relies on a faster-scanned primary beam. The brightness of the signal depends on the number of secondary electrons reaching the detector. If the beam enters the sample perpendicular to the surface, then the activated region is uniform about the axis of the beam and a certain number of electrons "escape" from within the sample. As the angle of incidence increases, the "escape" distance of one side of the beam will decrease, and more secondary electrons will be emitted. Thus steep surfaces and edges tend to be brighter than flat surfaces, which results in images with a well-defined, three-dimensional appearance. Using this technique, resolutions less than 1 nm are possible.

1.5.3.2 Detection of backscattered electrons

Backscattered electrons (BSE) consist of high-energy electrons originating in the electron beam that are reflected or back-scattered out of the specimen interaction volume. Backscattered electrons may be used to detect contrast between areas with different chemical compositions, especially when the average atomic number of the various regions is different, since the brightness of the BSE image tends to increase with the atomic number.

Backscattered electrons can also be used to form an electron backscatter diffraction (EBSD) image. This image can be used to determine the crystallographic structure of the specimen.

There are fewer backscattered electrons emitted from a sample than secondary electrons. The number of backscattered electrons leaving the sample surface upward might be significantly lower than those that follow trajectories toward the sides. Additionally, in contrast with the case with secondary electrons, the collection efficiency of backscattered electrons cannot be significantly improved by a positive

bias common on Everhart-Thornley detectors. This detector positioned on one side of the sample and has low collection efficiency for backscattered electrons due to small acceptance angles. The use of a dedicated backscattered electron detector above the sample in a "doughnut" type arrangement, with the electron beam passing through the hole of the doughnut, greatly increases the solid angle of collection and allows for the detection of more backscattered electrons.

1.5.3.3 Beam-injection analysis of semiconductors

The nature of the SEM's probe, energetic electrons, makes it uniquely suited to examining the optical and electronic properties of semiconductor materials. The high-energy electrons from the SEM beam will inject charge carriers into the semiconductor. Thus, beam electrons lose energy by promoting electrons from the valence band into the conduction band, leaving behind the holes.

In a direct band gap material, recombination of these electron-hole pairs will result in cathodoluminescence; if the sample contains an internal electric field, such as is present at a p-n junction, the SEM beam injection of carriers will cause electron beam induced current (EBIC) to flow.

Cathodoluminescence and EBIC are referred to as "beam-injection" techniques, and are very powerful probes of the optoelectronic behavior of semiconductors, particularly for studying nanoscale features and defects.

1.5.3.4 Cathodoluminescence

Cathodoluminescence (CL), the emission of light when atoms excited by high-energy electrons return to their ground state, is analogous to UV-induced fluorescence, and some materials such as zinc sulphide and some fluorescent dyes, exhibit both phenomena. Cathodoluminescence is most commonly experienced in

everyday life as the light emission from the inner surface of the cathode ray tube (CRT) in television sets and computer CRT monitors. In the SEM, CL detectors either collect all light emitted by the specimen, or can analyse the wavelengths emitted by specimen and display a spectrum or an image of cathodoluminescence in real colour.

1.5.3.5 X-ray microanalysis

X-rays, which are also produced by the interaction of electrons with the sample, may also be detected in an SEM equipped for energy-dispersive X-ray spectroscopy or wavelength in dispersive X-ray spectroscopy.

1.5.3.6 Resolution of the SEM

The spatial resolution of the SEM depends on the size of the electron spot, which in turn depends on both the wavelength of the electrons and the magnetic electron-optical system which produces the scanning beam. The resolution is also limited by the size of the interaction volume, or the extent to which the material interacts with the electron beam. The spot size and the interaction volume both might be large compared to the distances between atoms, so the resolution of the SEM is not high enough to image individual atoms, as is possible in the shorter wavelength (i.e. higher energy) transmission electron microscope (TEM). The SEM has compensating advantages, though, including the ability to image a comparatively large area of the specimen; the ability to image bulk materials (not just thin films or foils); and the variety of analytical modes available for measuring the composition and nature of the specimen. Depending on the instrument, the resolution can fall somewhere between less than 1 nm and 20 nm. In general, SEM images are easier to interpret than TEM images.

1.5.3.7 Procedure

Figure 1.10 shows the schematic diagram of a scanning electron microscope. A detailed explanation of how a typical SEM functions are as follows:

1) The "Virtual Source" at the top represents the electron gun, producing a stream of monochromatic electrons.

2) The stream is condensed by the first condenser lens (usually controlled by the "coarse probe current knob"). This lens is used to both form the beam and limit the amount of current in the beam. It works in conjunction with the condenser aperture to eliminate the high-angle electrons from the beam

3) The beam is then constricted by the condenser aperture (usually not user selectable), eliminating some high-angle electrons

4) The second condenser lens forms the electrons into a thin, tight, coherent beam and is usually controlled by the "fine probe current knob"

5) A user selectable objective aperture further eliminates high-angle electrons from the beam

6) A set of coils then "scan" or "sweep" the beam in a grid fashion (like a television), dwelling on points for a period of time determined by the scan speed (usually in the microsecond range)

7) The final lens, the Objective, focuses the scanning beam onto the part of the specimen desired.

8) When the beam strikes the sample (and dwells for a few microseconds) interactions occur inside the sample and are detected with various instruments

9) Before the beam moves to its next dwell point these instruments count the number of interactions and display a pixel on a CRT whose intensity is determined

by this number (the more reactions the brighter the pixel).

10) This process is repeated until the grid scan is finished and then repeated, the entire pattern can be scanned 30 times per second.

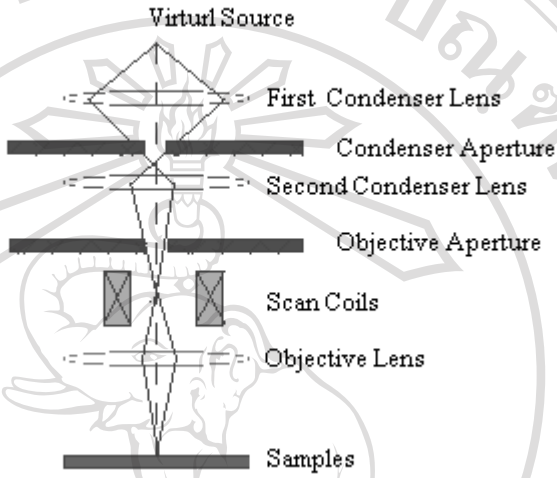

Figure 1.10 Schematic diagram of a scanning electron microscope [32]

1.5.4 Transmission Electron Microscopy (TEM) [30, 33-35]

The TEM is used heavily in both material science/metallurgy and the biological sciences. In both cases the specimens must be very thin and able to withstand the high vacuum present inside the instrument.

For biological specimens, the maximum specimen thickness is roughly 1 micrometre. To withstand the instrument vacuum, biological specimens are typically held at liquid nitrogen temperatures after embedding in vitreous ice, or fixated using a negative staining material such as uranyl acetate or by plastic embedding. Typical biological applications include tomographic reconstructions of small cells or thin sections of larger cells and 3-D reconstructions of individual molecules via Single Particle Reconstruction.

In material science/metallurgy the specimens tend to be naturally resistant to vacuum, but must be prepared as a thin foil, or etched so some portion of the specimen is thin enough for the beam to penetrate. Preparation techniques to obtain an electron transparent region include ion beam milling and wedge polishing. The focused ion beam (FIB) is a relatively new technique to prepare thin samples for TEM examination from larger specimens. Because the FIB can be used to micro-machine samples very precisely, it is possible to mill very thin membranes from a specific area of a sample, such as a semiconductor or metal. Materials that have dimensions small enough to be electron transparent, such as powders or nanotubes, can be quickly produced by the deposition of a dilute sample containing the specimen onto support grids. The suspension is normally in a volatile solvent, such as ethanol, ensuring that the solvent rapidly evaporates allowing a sample that can be rapidly analysed.

The imaging techniques explained below are particularly important in materials science. Faults in crystals affect both the mechanical and the electronic properties of materials, so understanding how they behave gives a powerful insight. By carefully selecting the orientation of the sample, it is possible not just to determine the position of defects but also to determine the type of defect present. If the sample is orientated so that one particular plane is only slightly tilted away from the strongest diffracting angle (known as the Bragg Angle), any distortion of the crystal plane that locally tilts the plane to the Bragg angle will produce particularly strong contrast variations. However, defects that produce only displacement of atoms that do not tilt the crystal to the Bragg angle (i.e. displacements parallel to the crystal plane) will not produce strong contrast.

Furthermore, the high resolution TEM (HRTEM) technique allows the direct observation of crystal structure and therefore has an advantage over other methods in that there is no displacement between the location of a defect and the contrast variation caused in the image. However, it is not always possible to interpret the lattice images directly in terms of sample structure or composition. This is because the image is sensitive to a number of factors (specimen thickness and orientation, objective lens defocus, spherical and chromatic aberration), and although quantitative interpretation of the contrast shown in lattice images is possible, it is inherently complicated and may require extensive simulation of the images. Computer modeling of these images has added a new layer of understanding to the study of crystalline materials.

1.5.4.1 Imaging in the TEM

The contrast in a TEM image is not like the contrast in a light microscope image. A crystalline material interacts with the electron beam mostly by diffraction rather than absorption, although the intensity of the transmitted beam is still affected by the volume and density of the material through which it passes. The intensity of the diffraction depends on the orientation of the planes of atoms in a crystal relative to the electron beam; at certain angles the electron beam is diffracted strongly from the axis of the incoming beam, while at other angles the beam is largely transmitted. Modern TEMs are often equipped with specimen holders that allow the user to tilt the specimen to a range of angles in order to obtain specific diffraction conditions, and apertures placed below the specimen allow the user to select electrons diffracted in a particular direction.

A high-contrast image can therefore be formed by blocking electrons deflected away from the optical axis of the microscope by placing the aperture to allow only unscattered electrons through. This produces a variation in the electron intensity that reveals information on the crystal structure, and can be viewed on a fluorescent screen, or recorded on photographic film or captured electronically.

This technique (known as Bright Field or Light Field) is particularly sensitive to extended crystal lattice defects in an otherwise ordered crystal, such as dislocations. As the local distortion of the crystal around the defect changes the angle of the crystal plane, the intensity of the scattering will vary around the defect. As the image is formed by the distortion of the crystal planes around the defect, the contrast in these images does not normally coincide exactly with the defect, but is slightly to one side.It is also possible to produce an image from electrons deflected by a particular crystal plane. By either moving the aperture to the position of the deflected electrons, or tilting the electron beam so that the deflected electrons pass through the centred aperture, an image can be formed of only deflected electrons, known as a Dark Field image.

In the most powerful diffraction contrast TEM instruments, crystal structure can also be investigated by High Resolution Transmission Electron Microscopy (HRTEM), also known as phase contrast imaging as the images are formed due to the differences in phase of electron waves scattered through a thin specimen.

Resolution of the HRTEM is limited by spherical and chromatic aberration, but a new generation of aberration correctors has been able to overcome spherical aberration. Software correction of spherical aberration has allowed the production of images with sufficient resolution to show carbon atoms in diamond separated by only

0.89 ångströms (89 pm, one ångström is 0.0000000001 of a meter or 100 picometers) and atoms in silicon at 0.78 ångströms (78 pm) at magnifications of 50 million times. Improved resolution has also allowed the imaging of lighter atoms that scatter electrons less efficiently. The ability to determine the positions of atoms within materials has made the HRTEM an indispensable tool for nanotechnology research and development in many other fields, including heterogeneous catalysis and the development of semiconductor devices for electronics and photonics.

1.5.4.2 Diffraction

In conventional electron diffraction the region of interest is selected by means of a physical aperture. The smallest area which can be selected by this technique is limited by the spherical aberration of the objective lens and is usually about 1 μm in diameter. By using the small probes obtainable either in 'nanoprobe' or scanning modes it is possible to select a smaller area of the specimen with the focused beam. This will give, depending on the convergence angle set by the condenser aperture, a micro-selected area diffraction pattern or a convergent beam diffraction pattern as shown in Figure 1.11 (a), (b).

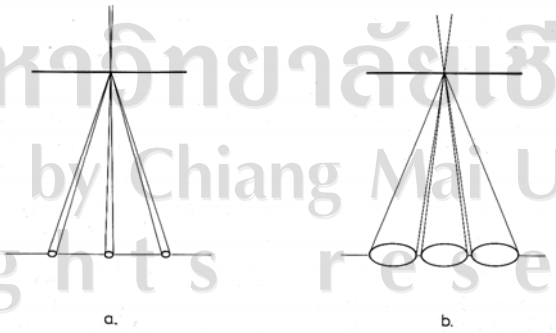

Figure 1.11 The approximate geometry of

(a) microdiffraction and (b) convergent beam diffraction.

The only significant difference is in the beam convergence angle at the specimen. [33]

1.5.4.3 Analysis

The two techniques of energy dispersive X-ray analysis (EDX) and electron energy loss analysis (EELS) are frequently available on TEM/STEM instruments. The first uses characteristic X-rays excited from the small volume of specimen irradiated by the beam, while the second detects the energy lost by electrons which have interacted with the specimen. The EDX detector is fitted to the side of the microscope close to the specimen, whereas the EELS spectrometer sits of the microscope close to the specimen. Both these types of analysis are useful and be able to define the analyzed region by focusing the beam onto a very small area using ‘nanoprobe’ or scanning modes.

1.5.4.4 Procedure

Figure 1.12 shows the schematic diagram of transmission electron microscope. The detailed explanation of how TEM functions are as follows:

1. The "Virtual Source" at the top represents the electron gun, producing a stream of monochromatic electrons.

2. This stream is focused to a small, thin, coherent beam by the use of condenser lenses 1 and 2. The first lens (usually controlled by the "spot size knob") largely determines the "spot size"; the general size range of the final spot that strikes the sample. The second lens (usually controlled by the "intensity or brightness knob" actually changes the size of the spot on the sample; changing it from a wide dispersed spot to a pinpoint beam.

3. The beam is restricted by the condenser aperture (usually user selectable), knocking out high angle electrons (those far from the optic axis, the dotted line down the center)

4. The beam strikes the specimen and parts of it are transmitted

5. This transmitted portion is focused by the objective lens into an image

6. Optional Objective and Selected Area metal apertures can restrict the beam; the Objective aperture enhancing contrast by blocking out high-angle diffracted electrons, the Selected Area aperture enabling the user to examine the periodic diffraction of electrons by ordered arrangements of atoms in the sample

7. The image is passed down the column through the intermediate and projector lenses, being enlarged all the way

8. The image strikes the phosphor image screen and light is generated, allowing the user to see the image. The darker areas of the image represent those areas of the sample that fewer electrons were transmitted through (they are thicker or denser). The lighter areas of the image represent those areas of the sample that more electrons were transmitted through (they are thinner or less dense)

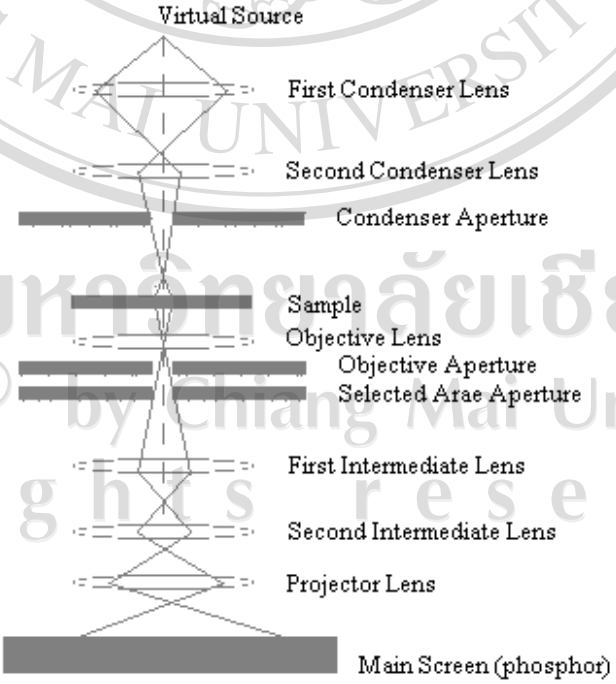

Figure 1.12 Schematic diagram of a transmission electron microscope [34]

1.5.5 The Brunauer-Emmett-Teller (BET) [36,37]

BET theory is a well-known rule for the physical adsorption of gas molecules on a solid surface. In 1938, Stephen Brunauer, Paul Hugh Emmett, and Edward Teller published an article about the BET theory in a journal for the first time; "BET" consists of the first initials of their family names.

1.5.5.1 BET theory

The Brunauer-Emmett-Teller method is base on non-specific physisorption of a gas (N_2 or Ar) onto a solid close to the condensation temperature of the adsorbing gas. Adsorption is characterized by an isotherm which represents the equilibrium amount of gas adsorbed on a solid at a given temperature as a function of pressure.

The concept of the theory is an extension of the Langmuir theory, which is a theory for monolayer molecular adsorption, to multilayer adsorption with the following hypotheses:

(a) gas molecules physically adsorb on a solid in layers infinitely

(b) there is no interaction between each adsorption layer

(c) the Langmuir theory can be applied to each layer.

The resulting BET equation is expressed by (1.7):

$$\frac{1}{V\left[(Po/P)-1\right]} = \frac{1}{V_m C} + \frac{C-1}{V_m C}\frac{P}{Po} \qquad (1.7)$$

Where:

P and P_0 are the equilibrium and the saturation pressure of adsorbates at the temperature of adsorption,

v is the adsorbed gas quantity (for example, in volume units)

v_m is the monolayer adsorbed gas quantity

c is the BET constant, which is expressed by (1.8):

$$C = \exp\left(\frac{E_1 - E_L}{RT}\right) \quad (1.8)$$

Where:

E_1 is the heat of adsorption for the first layer

E_L is that for the second and higher layers and is equal to the heat of liquefaction.

1.5.5.2 BET plot

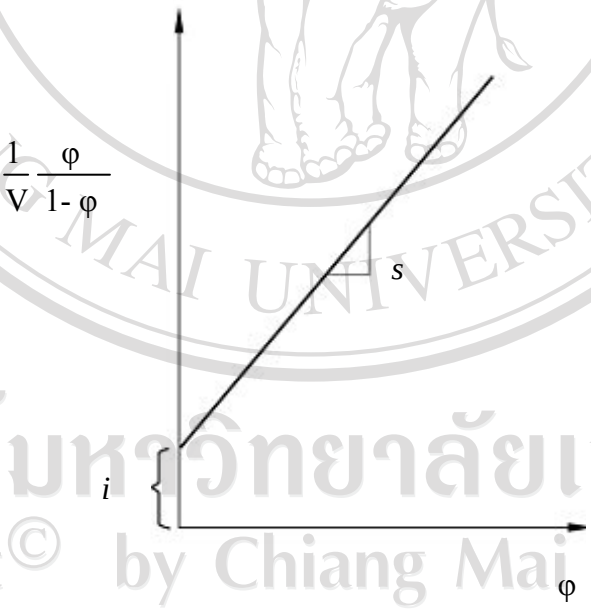

Figure 1.13 Typical BET plot [36]

Equation (1.7) is an adsorption isotherm and can be plotted as a straight line with $1 / V[(P_0 / P) - 1]$ on the y-axis and $\varphi = P / P_0$ on the x-axis according to experimental results. This plot is called a BET plot. The linear relationship of this equation is maintained only in the range of $0.05 < P / P_0 < 0.35$. The value of the slope s and the y-intercept i of the line are used to calculate the monolayer adsorbed gas quantity V_m and the BET constant C. The following equations can be used:

$$s = \frac{C-1}{V_m C} \tag{1.9}$$

$$i = \frac{1}{V_m C} \tag{1.10}$$

Solving the preceding equations for V_m and C gives

$$Vm = \frac{1}{s + i} \tag{1.11}$$

and

$$C = \frac{s}{i} + 1 \tag{1.12}$$

1.5.5.3 Surface area calculation

The BET method is widely used in surface science for the calculation of surface areas of solids by physical adsorption of gas molecules. A total surface area S_{total} and a specific surface area S are evaluated by the following equations:

$$S_{total} = \frac{V_m \overline{N} \sigma}{\overline{M}} \quad (1.13)$$

Where:

S_{total} is sample surface area

σ is the cross-sectional area

$\overline{M}$ is the molecular weight of an adsorbate molecule

$\overline{N}$ is the Avogadro's number

1.5.4.4 Particle Size (d_{BET})

The particle size (d_{BET}) is calculated by BET measurement using specific surface area (SSA) and density of sample by assuming that the particles do have spherical shape. The following equation can be used:

$$d_{BET} = \frac{6}{SSA_{BET} \rho_{sample}} \quad (1.14)$$

Where:

ρ_{sample} is the density of sample

1.6 Photocatalyst [24, 29, 38-43]

The photocatalyst is an environmental clean-up material that arises on the surface when absorb the light such as the sunlight or from fluorescent lamps, can remove such an organic compound.

1.6.1 Semiconductors as photocatalysts

The heterogeneous photocatalyst has been predicted properties by using band theory. Briefly, the band gap is the range of forbidden energies between non-overlapping bands and the band gap energy characterizes the band structure of a solid. Heterogeneous photocatalysis is a process involves the occurrence of a chemical reaction in the presence of an illuminated semiconductor. A semiconductor can act as a photocatalyst due to its specific electronic structure which is characterized by a filled valence band and an empty conduction band. Figure 1.14 shows the comparison among the band structure of metal, semiconductor, and insulator. The semiconductors are distinguished by the width of the energy gap. The allowable energies of electrons in a crystal are called the energy levels. In crystal with an atomic lattice, the neighboring nuclei influence the electronic structure and sharp energy levels (e.g. those associated with single atoms) become band of energy, each band representing specific quantum states. Forbidden bands exist between these bands. Electrons giving rise to chemical bonding constitute a valence band as shown in Figure 1.14.

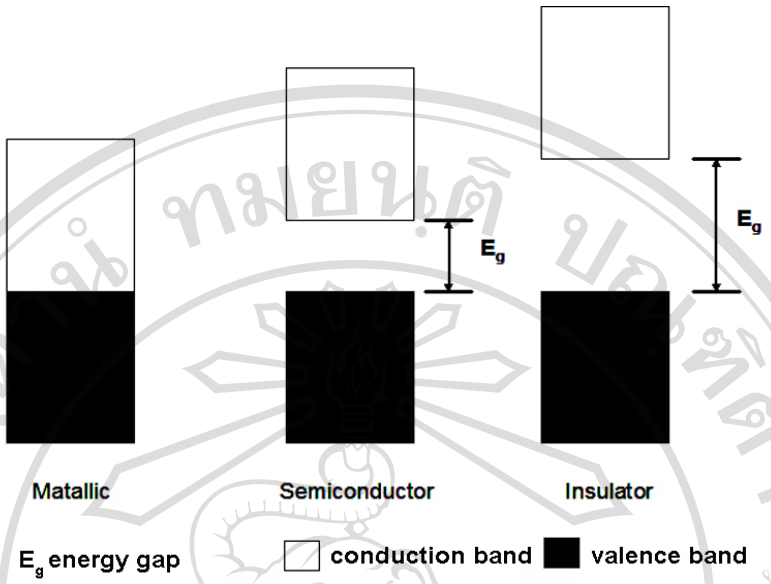

Figure 1.14 Energy band diagrams for metallic, semiconductor, and insulator [38]

The energy gap between valence band and conduction band of metallic solids are connected, therefore atoms are closely packed together. The characteristic properties of metallic conductor are high electrical and thermal conductivity, and high optical reflectivity. In the insulator has a wider band gap, hence the promotion of an electron from the valence band to the conduction band is difficult. The electrical conductivity of semiconductor is ordinarily much smaller than that of a metal due to the limited concentration of free electron and holes. The band gap of a semiconductor lies between a metallic solid and an insulator. Therefore, the promotion of electrons from the valence band to the conduction band, leaving holes in semiconductors, can be achieved easily relative to insulators and subsequently utilized during the photocatalytic process. In particular, SnO_2, with relatively large band gap energy of 3.5 to 3.6 eV as shown in Figure 1.15, can achieve a powerful oxidation-reduction reaction with the ultraviolet rays present in our living environment. It is known that

active oxygen and radical species existing in the presence of oxygen and water take part in the oxidation reduction reaction.

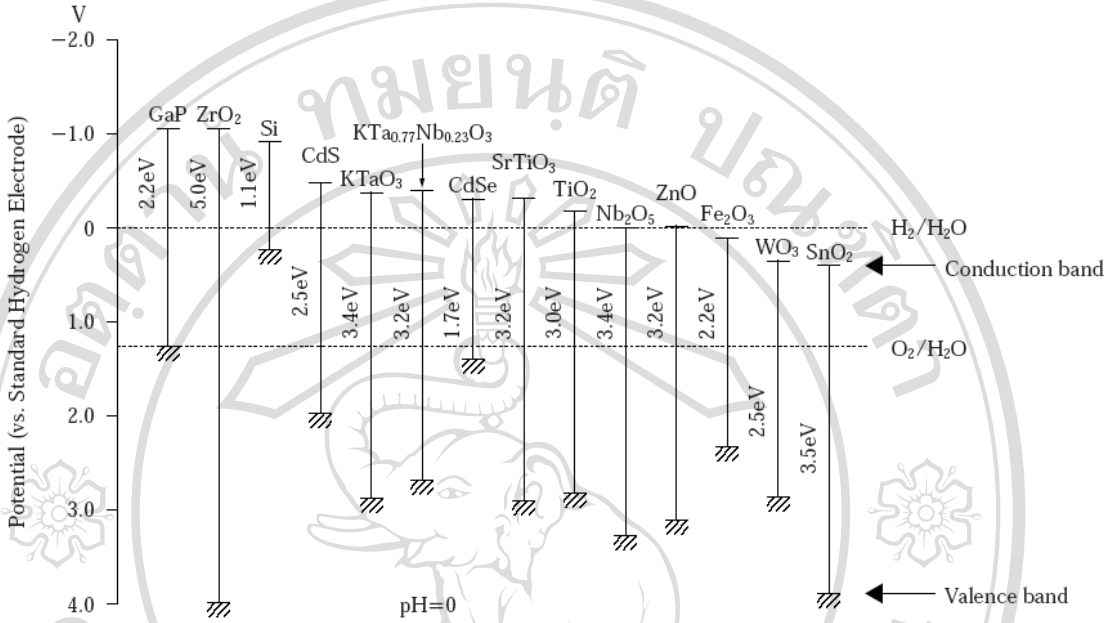

Figure 1.15 Energy structures of various photosemiconductors [24]

1.6.2 Principles

The photocatalyst works can be explained by the following principles.

1.6.2.1 Absorption of light

When photocatalyst absorbs a photon of light (hv) from sunlight or illuminated light source (fluorescent lamps), it will produce pairs of electrons and holes. The electron of the valence band of the photocatalyst becomes excited when illuminated by light. The excess energy of this excited electron promoted the electron to the conduction band therefore creating the negative-electron (e-) and positive-hole (h+) pair. This stage is referred as the semiconductor's photo-excitation state.

Thus, the energy that makes electrons jump up is provided by the light and this light energy is related to the light's wavelengths.

Therefore, calculating from the height that the electrons have to jump up, this light should have the same wavelength as ultraviolet light, relatively with the following equations.

$$E = h\nu \quad (1.15)$$

$$\nu = c/\lambda \quad (1.16)$$

Therefore $E = hc/\lambda$ (1.17)

Where:

E is energy

h is Plank's constant

ν is frequency

c is light speed

and λ is wavelength

1.6.2.2 OH radical appearance

With the effect of electrical field, electron e^- and hole h^+ are separated and moved to the surface of particle. According to energetic theory, h^+ can oxygenates OH^- and H_2O conglutinated on surface of photocatalyst and become a free radical.

The positive-hole of photocatalyst breaks apart the water molecule to form hydrogen gas and hydroxyl radical. The negative-electron reacts with oxygen molecule to form superoxide radicles ($^{\bullet}O_2^-$). This cycle continues when light is available. This is an overall mechanism of photocatalytic reaction of photocatalytic oxidation

The most powerful advanced oxidation systems are based on the generation of hydroxyl radicals (•OH). The hydroxyl radical is an extremely powerful oxidation agent. Table 1.3 shows a list of common chemical oxidants, placed in the order of their oxidizing strength.

Table 1.3 Lists of common chemical oxidants in the order of their relative power [40]

Relative Power of Chemical Oxidation		
Compound	**Oxidation Potential (Volts)**	**Relative Oxidizing Power (Cl_2=1.0)**
Hydroxyl Radical	2.80	2.10
Sulfate Radical	2.60	1.90
Ozone	2.10	1.50
Hydrogen Peroxide	1.80	1.30
Permanganate	1.70	1.20
Chlorine Dioxide	1.50	1.10
Chlorine	1.50	1.00
Oxygen	1.20	0.90
Bromine	1.10	0.80
Iodine	0.76	0.54

1.6.2.3 Mineralization of organic compound

•OH radical takes the electron by the strong oxidation from the nearby organic compounds to become stable. The organic compound is decomposed by loss of the electron and finally becomes carbon dioxide and water, and emanated to an atmosphere.

According to energetic theory, h+ can oxygenates OH^- and H_2O conglutinated on surface of photocatalyst into free radical. Moreever, free radical has strong oxidation ability and can oxygenate and decompose various organic compound,

bacteria and part of inorganic contamination into harmless substances: CO_2 and H_2O. $^{\bullet}OH$ radical has no selectivity to reactant, so it makes crucial effect in photocatalyzing. Meanwhile, high active electron e- has strong deoxidized ability and can deoxidize oxygen in air.

Utilizing the strong oxidation strength of hydroxyl radical, photocatalytic oxidation can effectively disinfect, deodorize, and purify air, water, and different surface area. Figure 1.16 shows the schematic diagram the principle of photocatalytic process.

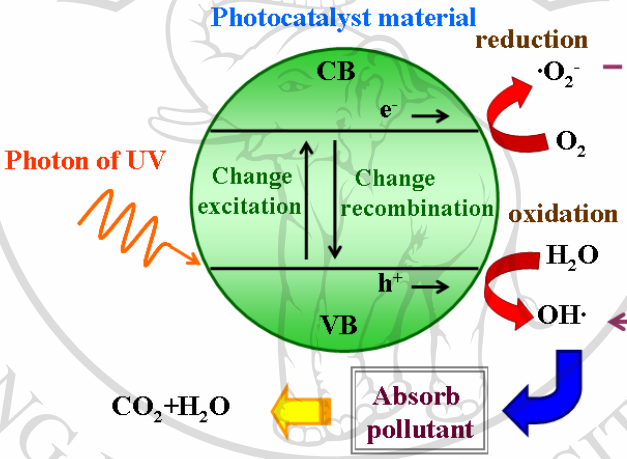

Figure 1.16 Simplified diagram of the mechanism for mineralization of photocatalyst [41]

Steps of photocatalyst reaction for degradation of organic compound were shown as following:

1. Electron-hole pair generation

$SnO_2 \rightarrow SnO_2 (e^-_{cb}, h^+_{vb}) \rightarrow$ recombination (1.18)

2. Possible traps for holes

(a) Surface adsorbed water molecules

$SnO_2 (h^+_{vb})+H_2O_{ads} \rightarrow SnO_2+OH^{\cdot}_{ads}+H^+$ (1.19)

$SnO_2 (h^+_{vb})+H_2O_{ads} \rightarrow SnO_2 +1/2O_2$ (1.20)

(b) Surface adsorbed hydroxyl ions

$SnO_2\ (h^+_{vb})+OH^-_{ads} \rightarrow SnO_2 + OH^{\cdot}_{ads}$ (1.21)

(c) Electron donor D species

$SnO_2\ (h^+_{vb})+D_{ads} \rightarrow SnO_2+D^+_{ads}$ (1.22)

3. Possible traps for electrons

$SnO_2\ (e^-_{cb})+O_{2ads}+H^+ \rightarrow SnO_2+OH^{\cdot}{}_2 \leftrightarrow {}^{\cdot}O^-_2+H^+$ (1.23)

$OH^{\cdot}{}_2+ SnO_2\ (e^-_{cb})+ H^+ \rightarrow SnO_2+ H_2O$ (1.24)

$2OH^{\cdot}{}_2 \rightarrow H_2O_2+O_2$ (1.25)

$H_2O_2+ {}^{\cdot}O^-_2 \rightarrow OH^{\cdot}+O_2+OH^-$ (1.26)

$H_2O_2+h\nu \rightarrow 2OH^{\cdot}$ (1.27)

$H_2O_2+ SnO_2\ (e^-_{cb}) \rightarrow SnO_2+OH^{\cdot}+OH^-$ (1.28)

$SnO_2\ (e^-_{vb})+A_{ads} \rightarrow SnO_2+A^+_{ads}$ (1.29)

4. Recombination

$SnO_2\ (e^-_{cb}+h^+_{vb}) \rightarrow SnO_2+energy$ (1.30)

1.6.3 Application of photocatalyst

1.6.3.1 Anti-bacteria

Photocatalyst does not only kill bacteria cells, but also decompose the cell itself. The photocatalyst has been found to be more effective than any other antibacterial agent, because the photocatalytic reaction works even when there are cells covering the surface and while the bacteria are actively propagating. The end toxin produced at the death of cell is also expected to be decomposed by the photocatalytic action.

1.6.3.2 Deodorization

On the deodorizing application, the hydroxyl radicals accelerate the breakdown of any volatile organic compounds or VOCs by destroying the molecular bonds. This will help combine the organic gases to form a single molecule that is not harmful to human thus enhance the air cleaning efficacy. Some of the examples of odor molecules are: Tobacco odor, formaldehyde, nitrogen dioxide, urine and fecal odor, gasoline, and many other hydrocarbon molecules in the atmosphere.

1.6.3.3 Air purification

The photocatalytic activity can be applied for the reduction or elimination of polluted compounds in air such as NO_x, cigarette smoke, as well as volatile compounds arising from various construction materials. Also, high photocatalytic activity can be applied to protect lamp-houses and walls in tunneling, as well as to prevent white tents from becoming sooty and dark. Atmospheric constituents such as chlorofluorocarbons (CFCs) and CFC substitutes, greenhouse gases, and nitrogenous and sulfurous compounds undergo photochemical reactions either directly or indirectly in the presence of sunlight. In a polluted area, these pollutants can eventually be removed.

1.6.3.4 Anti fogging and self-cleaning

Most of the exterior walls of buildings become soiled from automotive exhaust fumes, which contain oily components. When the original building materials are coated with a photocatalyst, a protective film provides the self-cleaning building by becoming antistatic, super oxidative, and hydrophilic. The hydrocarbon from automotive exhaust is oxidized and the dirt on the walls washes away with rainfall, keeping the building exterior clean at all times.

1.6.3.5 Water purification

Photocatalyst coupled with UV lights can oxidize organic pollutants into nontoxic materials, such as CO_2 and water and can disinfect certain bacteria. This technology is very effective at removing further toxic organic compounds (TOCs) and at killing a variety of bacteria and some viruses in the secondary wastewater treatment. Pilot projects demonstrated that photocatalytic detoxification systems could effectively kill fecal coli form bacteria in secondary wastewater treatment.

1.7 Modified photocatalysts: enhancement of photocatalytic activity [44-46]

Interfacial charge transfer in the reactions when occurs could enhance the photoactivity. Improved charge separation and inhibition of charge carrier recombination is essential in improving the overall quantum efficiency for interfacial charge transfer. This can be achieved by modifying the properties of the particles by a selective surface treatment.

1.7.1 Doping with transition metal ions

The performance of photocatalysts can be changed by doping with the transition metal ions into semiconductors. The dynamics of electron-hole recombination and interfacial charge transfer will be affected. While some studies have shown that doping with transition metal ion into semiconductors can be effective in lengthening the lifetime of the generated charge carriers. The dopant ions may be adsorbed on the surface, or incorporated into the interior of the particle upon firing, or they may form separate oxide phases. The dopant ions can function as both hole and electron trap or they can mediate interfacial charge transfer. Once incorporated into the interior of semiconductors, the dopant ions may occupy either lattice substitutional

or interstitial sites. Their ability to function as trap site and/or to mediate interfacial charge transfer will depend on these factors. Finally, the site where the electron gets trap greatly influences the redox chemistry of the doped semiconductor. However, if an electron is trapped in a deep trapping site, it will have a longer lifetime, but it may also have a lower redox potential. This might result in a decrease in the photoreactivity.

1.7.2 Metal ion deposition

Metal ions deposition onto semiconductors, mostly noble metals due to noble metal can enhance the reaction of photocatalysis, on the surface of the photocatalyst is also utilized enhance the separation of electron-hole pairs. When metal ion deposition on semiconductor, it can change the semiconductor surface properties. Figure 1.17 illustrates the metal ion in contact with surface of semiconductor. Upon excitation, electron can migrate to the deposit metal where they can be trapped or captured by an oxidant (A^+-electron acceptor). The hole is then free to migrate to the surface where oxidation can be occur (D (electron donor) $\rightarrow D^+$).

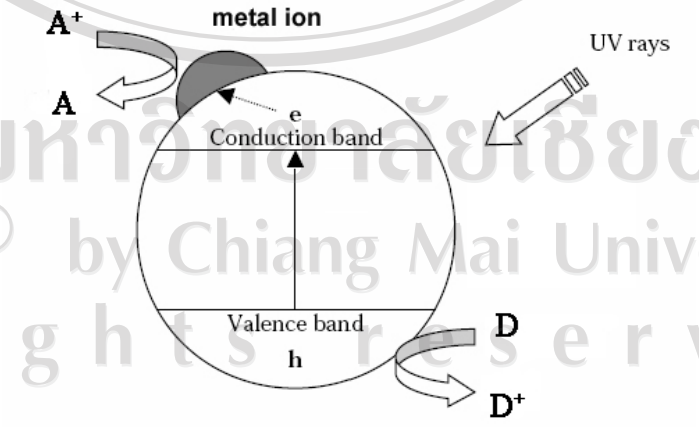

Figure 1.17 Electron mediation by metal ion in contact with semiconductor surface [45]

1.7.3 Coupled semiconductors

In a coupled semiconductor system the two particles are in contact with each other and both holes and electrons are accessible on the surface for selective oxidation and reduction processes. The possessing different energy levels for their corresponding conduction and valence bands, provides an approach to achieve a more efficient charge separation, an increased lifetime of the charge carriers and an enhanced interfacial charge transfer to adsorbed substrates. An interesting approach to prevent electron-hole recombination is the coupling of two semiconductor catalyst to improve charge separation. This strategy accomplishes vector displacement of charges on the semiconductors and reduces electron-hole recombination. Thus, coupled semiconductor systems offer potential advantages for solar energy utilization because of the possibilities presented by inter-particle electron transfer.

1.7.4 Application of nano-sized particles

Nano-sized of particle to a certain "critical size" produces the so-called quantum size effects (Q-size). Quantum-size effects occur when the particles size of the semiconductor smaller than Bohr radius of the first excitation state. One of the most detached effects of reducing the size of a particle to that of quantum size is increase band gap energy. The band gap energy can be increased because as the particle size approaches that of nano-sized, the photogenerated electron and hole cannot fit into such as a particle unless they assume a state of higher kinetic energy. There seem to be many discrepancies in the reported quantum size of nanoparticle possibly due to the different crystalline phases of the particles.

1.8 Literature review

In 2000, oxidation of methane and carbon monoxide was carried out on silver/ceria composite oxide prepared by co-precipitation, and the behavior of the lattice oxygen of silver were investigated by Imamura *et al*.[47]. In the high temperature oxidation of methane, silver (I) oxide decomposed and aggregated to large particles of metallic silver and rapidly deactivated. On the other hand, silver retained high activity during the low temperature oxidation of carbon monoxide. It was found, however, that ceria accelerated the desorption of the lattice oxygen of silver, which was assumed to be related to the well known oxygen storage function of ceria. Although silver tended to be converted more easily to metallic state in the presence of ceria, the function of ceria of sustaining the dispersed state of silver will helped to maintain the high activity of the latter in the oxidation of carbon monoxide.

In 2001, the results from a study on the photocatalytic decomposition of water to oxygen over pure WO_3, CeO_2, and TiO_2 were reported by Bamwenda *et al*.[48]. It has been demonstrated that Fe^{3+} and Ce^{4+} species were efficient electron acceptors during the photoproduction of O_2 over a variety of oxides, even at very low concentrations. The O_2 yield was found to depend on the type and surface activity of the cation used as an electron acceptor, and the salt counter anion. While Ce^{4+} gives slightly higher initial O_2 rates, Fe^{3+} tended to give higher long-term O_2 yields. The O_2 yield was found to be mainly sensitive to the intrinsic properties of a given material, such as the type of the oxide used and its physicochemical characteristics, e.g. crystal structure and level of crystallinity. For the powders tested, O_2 production was independent of the BET surface area and the activity did not correlate directly with the onset of light absorption of the powders. With a light having $\lambda \geq 330$ nm, O_2

production activity decreased in the order TiO_2-rutile > TiO_2-anatase > WO_3 > CeO_2 〉〉 amorphous TiO_2, whereas with a light having $\lambda \geq 420$ nm, it decreased in the order of WO_3 > TiO_2 > CeO_2. Small amounts of Sn on TiO_2-rutile markedly improved its activity. In addition, the O_2 yield strongly depended on the concentration of the electron acceptor and the pH of the suspension. During the reaction, small amounts of hydrogen were also produced. The reaction pathways for electron scavenging by Ce^{4+} and Fe^{3+}, and the process leading to O_2 evolution were discussed.

In 2002, the combustion synthesized Ag/CeO_2 catalysts were characterized by Extended X-ray Absorption Fine Structure (EXAFS) spectroscopy at the Ag K-edge as reported by Sarode *et al*.[49]. It has been found that Ag^+ like species was present in 1% Ag/CeO_2 catalyst, whereas mostly Ag metal clusters were found in 3% Ag/CeO_2. The analysis of EXAFS spectra indicated that about one oxygen atom was coordinated to Ag central atom at a distance of 2.19 Å in 1% Ag/CeO_2 catalyst along with eight coordinated Ag-Ag bond at 2.86 Å. The Ag-O bond was absent in 3% Ag/CeO_2.

In 2004**,** the nano-CeO_2/ZnO catalysts prepared using a novel combination of homogeneous precipitation with micro-emulsion for oxidative coupling of methane with CO_2 as an oxidant were reported by He *et al*.[50]. The prepared catalysts were compared with those prepared using the conventional impregnation. The catalysts prepared in two ways were characterized with FTIR, TEM, XRD and CO_2-TPD. The effects of the reaction temperature, the amount of ZnO doped in the catalysts and the average size were investigated. The experimental investigation demonstrated that methane conversion over the nano-CeO_2/ZnO catalysts prepared by the combined technique was higher than that obtained over catalysts prepared by the conventional

impregnation method.

In 2004, the CeO_2 nanoparticles were synthesized by homogeneous precipitation in alcohol/water mixed solvents by Chan *et al*. [1]. Six alcohols, including methanol, ethanol, n-propanol, iso-propanol, tert-butanol, and ethylene glycol (EG), were separately mixed with water as the solvents. The effects of nature and composition of alcohol on the resultant CeO_2 nanoparticles were under investigation. From the experimental results, it was found that the CeO_2 nanoparticles obtained from alcohol/water mixed solvent were primary particles confirmed by quite good consistency in the particle sizes from TEM, XRD and BET analyses. The results also revealed that the CeO_2 nanoparticles were non-porous. Besides, no matter what kind of alcohol was used, the prepared CeO_2 nanoparticles exhibited cubic fluorite structures. In pure water environment, the size of CeO_2 particles was about 15 nm, whereas it reduced to about 7 nm in the 67% ethanol/water solution. Especially in the EG/water solvent system, the resultant samples were extremely smaller than those in other systems. As the vol.% of alcohol increased, the particle size decreased for all solvent systems, and the reverse, the specific surface area increased. This alteration in particle size could be approximately interpreted by the changes in electrostatic interactions and nucleation rate with varying the dielectric constant of the mixed solvent.

In 2004, the synthesis of 20 mol% Gd_2O_3-doped CeO_2 solid solution (20 GDC) nano-particles via carbonate co-precipitation were reported by Tok *et al*.[51]. Precursors and calcined particles were characterized using TGA, XRD, BET, FESEM, and TEM. From the diffraction pattern using XRD with TEM, it was shown that the Gd^{3+} replaced the Ce^{4+} lattice in the fluorite structure (FCC) of CeO_2,

as opposed to it being a second phase in the CeO_2 structure. The 20 GDC particles were calcined at 700 ^oC for 2h, and sintered to >99% density at a very low sintering temperature of 1150 ^oC for 4h.

In 2005, nanocrystalline CeO_2 particles were firstly prepared by two-stage non-isothermal precipitation, i.e. precipitating at 70 ^oC and aging at another temperature by Chen *et al.*[7]. Experimental results showed that the intermediates at the end of precipitation stage were needle-like mixtures of Ce^{3+}-Ce^{4+} compounds. The subsequent aging temperature played an important role on the shape and size of final products. As the aging temperature suddenly reduced to 0 ^oC, the resultant particles retained their original needle-like structure via the topotactic mechanism, which could not be obtained by isothermal precipitation. As raising the aging temperature above 50 ^oC, the products were hexagonal and grown up with increasing temperature via the dissolution-recrystallization mechanism. Moreover, all products were cubic-fluorite structured CeO_2 with negligible Ce^{3+} content. As compared to the nanohexagons (aged at 90 ^oC), the nanoneedles (aged at 0 ^oC) exhibited an unordinary red shift in the UV absorption and possessed a smaller bandgap energy.

In 2005, nanoparticles of CeO_2 doped with 10 mol% of RE_2O_2 (RE = Sm and Gd) were synthesized by Li *et al.*[52], via the homogeneous precipitation method, employing nitrates as the starting salts and hexamethylenetetramine as the precipitant. Characterizations of the powders were achieved by elemental analysis, X-ray diffractometry (XRD), differential thermal analysis / thermogravimetry (DTA/TG), field-emission scanning electron microscopy (FE-SEM), and Brunauer–Emmett-Teller (BET). Sinterability of the powders was studied in air via dilatometry and isothermal sintering. Lightly hydrated crystalline solid solutions with the pre-determined

stoichiometry were formed directly during precipitation, as shown by the above characterization techniques and a leaching test with hydrochloric acid. The maximum doping level achieved by this synthetic procedure was found to be ~22 at.% for Sm^{3+} and ~24.4 at. % for Gd. The best annealing temperature for the powders intended for sintering was 400 ^{o}C, at which major dehydration occurred without significant crystallite growth and hard-aggregates formation. Fully dense ceramics (>99%) with ultrafine microstructures (~117–134nm) were fabricated via pressureless sintering for 4h at a low temperature of 1000^{o}C.

In 2005, well-densified 10 mol% Dy_2O_3-doped CeO_2 (20 DDC) ceramics with average grain sizes of ~0.12–1.5 μm were fabricated by pressureless sintering at 950–1550 ^{o}C using a reactive powder thermally decomposed from a carbonate precursor as reported by Wang *et al.*[53]. 20 DDC was synthesized via a carbonate coprecipitation method employing nitrates as the starting salts and ammonium carbonate as the precipitant. Electrical conductivity of the ceramics, measured by the dc three-point impedance method, shows a V-shape curve against the average grain size. The sample with the smallest grain size of 0.12 μm exhibited a high conductivity of ~$10^{-1.74}$ S/cm at the measurement temperature of 700 ^{o}C, which was about the same conduction level of the micro-grained 10 mol% Sm_2O_3- or Gd_2O_3-doped CeO_2, two leading electrolyte materials.

In 2006, the homogeneous and pure La-hexaaluminate catalyst was synthesized by the modified precipitation method, with buffer solution of NH_4HC0_3/NH_40H as the precipitant as reported by Meisheng *et al.*[54]. The hexaaluminate was formed at a low temperature of 1050 ^{o}C, and the hexaaluminate crystal phase was completely shaped by the temperature of 1200 ^{o}C. Transition

metal Mn occupied the position of hexaaluminate structure easily, which promoted crystal phase formation. The Ce introduction could improve the catalytic activity of hexaaluminate , which was hard to enter into the hexaalumiante structure, for existing as the CeO_2 with high oxygen storage capacity. The CeO_2 could offer influent active crystal oxygen, which also enhanced the redox performance of Mn. The activity of $LaMAl_{11}O_{19}$ (M = MnCe) was improved largely because of the synergic effect between Mn and Ce . When Mn atomic substituted amount for A1 was 2, the activity of $LaMn_xA1_{12-x}0_{19}$ was the best, with high redox performance.

In 2006, formation and thermal decomposition of rare earth (RE=La,Ce,Pr) hydroxides and oxides by homogeneous precipitation using hexamethylenetetramine were reported by Ozawa *et al.*[55]. The precipitatates were examined using thermal gravimetry and differential thermal analysis, infrared spectrometry and X-ray diffraction. The as-precipitated powders from the present process were $La(OH)_3$, CeO_2, $Pr(OH)_3$. In the case of Ce, a cubic fluorite phase of cerium dioxide was directly obtained. The lanthanum trihydroxide decomposed to oxides via three steps. Two-step dehydration decomposition behavior at 340 and 500°C was observed as $La(OH)_3 \rightarrow LaOOH + H_2O$ and $2LaOOH \rightarrow La_2O_3 + H_2O$. The activation energy (ΔH) for dehydration was 240 and 244 kJ/mol, respectively. The additional decomposition of carbonate-containing species was observed at 670°C with ΔH of 390 kJ/mol. $Pr(OH)_3$ did not show additional TGA profile of carbonate decomposition. Since no carbonate species formed in solution during the HMT (hexamethylenetetramine) precipitation (hydrolysis of this molecule), the difference between La and Pr depended on the strength of basicity in the reaction with CO_2 after precipitation.

In 2007, CeO_2 nanocrystalline was reported as a final decomposition product of hydrated cerium carbonate formed by using ammonium bicarbonate as precipitant by Zhai *et al*.[6]. The decomposition course of hydrated cerium carbonate and the formation process of CeO_2 were studied by TG and XRD. Moreover, the effect of the dispersant on the dispersity of the CeO_2 powder was studied by SEM. The results showed that hydrated cerium carbonate completely decomposed to CeO_2 at 300°C for 2h, and the crystallinity increased with increasing calcination temperature. The dispersity of the CeO_2 powder could be improved by the dispersant. For the first time, CeO_2 nanocrystalline was utilized as a photocatalyst for the photocatalytic degradation and decolorization of the dye Acidic Black 10B. The decolorizing rate could reach about 97% under appropriate conditions. Therefore, CeO_2 nanocrystalline possesses photocatalytic activity, and showed promising in dye wastewater treatment.

In 2007, Iridium catalysts were evaluated for the preferential CO oxidation under excess H_2 conditions (PROX) by Huang *et al*.[56]. The effects of various parameters including preparation methods, different oxides as supports, pretreatment process, content of Ir as well as reacting gas compositions on the catalytic performances were investigated. The results showed that both homogeneous deposition precipitation (HDP) and deposition precipitation (DP) methods could yield highly active Ir/CeO_2 catalysts, attributed to their satisfactory elimination of chlorines. Iridium was also deposited on various oxide supports (CeO_2, TiO_2, Al_2O_3 and MgO) by HDP method and only the Ir/CeO_2 catalyst exhibited excellent performance in PROX process. Reductive pretreatment of the Ir/CeO_2 (HDP) was found to be essential for obtaining the high activity. The best catalytic performance was obtained for the sample containing 1.60 wt% iridium. The presence of water in the feed had a

negligible influence on the total activity for CO_2 formation ; however, the presence of CO_2 negatively affected the catalytic performance of the Ir/CeO_2 (HDP). Additionally, the good stability of the Ir/CeO_2 catalyst made it a promising candidate for PROX process.

In 2007, Co_3O_4/CeO_2 mixed oxides were prepared by coprecipitation–oxidation, homogeneous precipitation, and complexation–combustion methods as reported by Jianiun *et al.*[57]. The catalysts were used to catalyze low-temperature CO oxidation under dry and humid conditions. The Co_3O_4/CeO_2 catalyst that was prepared by the coprecipitation–oxidation method followed by calcination at 538 K exhibited excellent activity and good resistance to water vapor poisoning. Remarkably, CO conversion of 99% was achieved at a temperature as low as 196 K and was maintained for more than 400 min under dry condition. When the reaction was carried out at 298 K, CO conversion of 94% was obtained after running the reaction for 2400 min. Even when 3.1% steam was added, CO conversion of 79% could be maintained after O and CeO_2 was closely related to the preparation 2400 min time-on-stream at 383 K. It was suggested that the strong interaction between Co_3O_4 and CeO_2 was closely related to the preparation route and calcination temperature and played a crucial role in the CO oxidation over the Co_3O_4/CeO_2 catalysis.

In 2007, a new bimetallic catalyst ($AgCo/CeO_2$) was studied for simultaneously catalytic removal of NO and CO in the absence or presence of O_2 by Zhang *et al.*[58]. CeO_2 prepared by homogeneous precipitation method was optimized as supports for the active components. The addition of Ag on CeO_2 greatly improved the catalytic activities in the lower temperature regions (≤ 300 ^{o}C), and the

introduction of Co on CeO_2 increased the activities at higher temperatures ($\geq 250\ ^oC$). The bimetallic Ag-Co/CeO_2 catalyst combined the advantages of the corresponding individual metal supported catalysts and showed superior activity due to the synergetic effect. The effect of support, temperature, loading amount, GHSV and oxygen on catalysis were investigated. NO and CO could be completely removed in the temperature range of 200-600 ^oC at a very high space velocity of 120000 h^{-1}. No deactivation was observed over 4% Ag-0.4% Co/CeO_2 catalyst even after 50 h test.

In 2008**,** a new catalyst composed of nickel oxide and cerium oxide was reported with respect to its activity for NO reduction by CO under stoichiometric conditions in the absence as well as the presence of oxygen by Wang *et al.*[59]. Activity measurements of the NO/CO reaction were also conducted over NiO/γ-Al_2O_3, NiO/TiO_2, and NiO/CeO_2 catalysts for comparison purposes. The results showed that the conversion of NO and CO were dependent on the nature of supports, and the catalysts decreased in activity in the order of NiO/CeO_2 > NiO/γ-Al_2O_3, >NiO/TiO_2. Three kinds of CeO_2 were prepared and used as support for NiO. They were the CeO_2 prepared by (i) homogeneous precipitation(HP), (ii) precipitation(PC), and (iii) direct decomposition(DP) methods. It was found that the NiO/CeO_2(HP) catalyst was the most active, and complete the conversion of NO and CO occurred at 210 ^oC at a space velocity of 120,000 h^{-1}.

1.9 Objective of the study

1.9.1 To synthesize CeO_2 nanoparticles by the homogeneous precipitation method

1.9.2 To synthesize Ag-doped CeO_2 nanoparticles by the impregnation method

1.9.3 To characterize pure CeO_2 and Ag-doped CeO_2 nanoparticles

1.9.4 To study the effect on photocatalytic activity of silver doping and dopant (Ag) concentration of CeO_2 nanoparticles